

Electronic Supplementary Information

Plasmonic Ge-Doped ZnO Nanocrystals

Enrico Della Gaspera,^{*a} Noel W. Duffy,^b Joel van Embden,^a Lynne Waddington,^a Laure Bourgeois,^c Jacek J. Jasieniak^{*a‡} and Anthony S. R. Chesman^{*a}

^a CSIRO Manufacturing Flagship Ian Wark Laboratories, Bayview Ave, Clayton, Victoria 3168, Australia. E-mail: enrico.dellagaspera@csiro.au (E.D.G.), jacek.jasieniak@monash.edu (J.J.J.), anthony.chesman@csiro.au (A.S.R.C.).

^b CSIRO Energy Flagship, Ian Wark Laboratories, Bayview Ave, Clayton, Victoria 3168, Australia.

^c Monash Centre for Electron Microscopy and Department of Materials Science and Engineering, Monash University, Wellington Road, Clayton, Victoria 3800, Australia.

[‡] Present address: Materials Science and Engineering, Monash University, Wellington Rd, Clayton, Victoria 3800, Australia.

Experimental

Materials

Zinc stearate (ZnSt_2 , technical) was supplied by BDH-Prolabo. 1-Dodecanol (DDOL, 99%), GeO_2 (99.99 %), glycolic acid (GlyH_2 , 99 %), 1-octadecene (ODE, 90%), oleic acid (OA, 90%), $\text{SnCl}_4 \cdot 5\text{H}_2\text{O}$ (98 %) and tetraethyl orthosilicate (TEOS, 99 %) were supplied by Sigma-Aldrich. Acetone (99.8%), ethanol (99.9%), tetrachloroethylene (TCE, 99%) and toluene (99.9%) were purchased from Merck. Oleylamine (OLA, >50 %) was supplied by TCI. Diaquabis(glycolato-O,O')germanium(IV) ($[\text{Ge}(\text{gly})_2(\text{H}_2\text{O})_2]$) was prepared according to a literature synthesis.^{1,2} All chemicals were used without further purification.

Synthesis

Ge precursor solution: $[\text{Ge}(\text{gly})_2(\text{H}_2\text{O})_2]$ (0.5 g, 2.0 mmol) was suspended in OLA (10 ml), which was subsequently heated to 120 °C under vacuum (8×10^{-2} mbar) for 30 min to yield a transparent solution. After standing at room temperature for a number of days the solution became slightly cloudy. Prior to use the solution was gently heated to return it to a homogeneous, transparent state.

Ge-doped ZnO nanocrystal synthesis (ZnO:Ge): $\text{Zn}(\text{St}_2)$ (2.83 g, 4.48 mmol), DDOL (7.2 g, 38.6 mmol), OA (3.96 g, 14.02 mmol), ODE (12 ml) and Ge precursor solution (4.5 ml) were added to a 250 ml three-neck flask. The solution was heated to 30–40 °C and degassed under vacuum (8×10^{-2} mbar) for 5 min. The reaction solution was then placed under an atmosphere of nitrogen and heated to 140 °C over a 15 min period, with the temperature then maintained for a further 30 min, giving a transparent, yellow-colored solution. The reaction temperature was then increased to 230 °C over a 20 min period. After approximately 5 min at 230 °C the reaction solution turned green-blue and slightly opaque. After heating at 230 °C for 2 hr, the reaction solution was removed from the heating mantle and allowed to cool to room temperature naturally. The reaction solution was then transferred to centrifuge tubes with the aid of a small amount of toluene, and diluted to a total volume of 80 ml with acetone to aid in flocculation prior to precipitation by centrifugation (4400 rpm, 4 min). The precipitate was redissolved in TCE (10 ml), and then acetone (20 ml) and ethanol (10 ml) were added to aid in flocculation prior to another precipitation by centrifugation (4400 rpm, 4 min). This final dissolution/precipitation step could be repeated to further remove unreacted reagents and purify the nanocrystals. The above instructions apply for the synthesis of nanocrystals with a 20 % nominal Ge doping level with respect to Zn. Lower nominal Ge doping levels of 8, 5, 2.5 and 1 % were achieved by using a lower proportion of the Ge precursor solution and adding neat OLA to ensure the volume of OLA (4.5 ml) remained consistent for each reaction. Ge free ZnO nanocrystals were synthesised using the above method with the Ge precursor solution completely substituted by neat OLA. The samples are labelled ZGeX, where X is the nominal doping level (*i.e.* Ge/Zn) expressed in atomic %.

Si doped ZnO nanocrystal synthesis (ZnO:Si): A stock solution of Si precursor was first prepared by adding TEOS (0.455 g, 2.2 mmol) to ODE (10 ml). The ZnO:Si nanocrystal synthesis then proceeded as for the above ZnO:Ge nanocrystal synthesis with the following reagents: Zn(St₂) (2.83 g, 4.48 mmol), DDOL (7.2 g, 38.6 mmol), OA (3.96 g, 14.02 mmol), OLA (4.5 ml), ODE (11 ml) and Si precursor solution (1 ml). The nominal doping level was 5%, and the sample has been labelled ZSi5.

Sn doped ZnO nanocrystal synthesis (ZnO:Sn): A stock solution of Sn precursor was first prepared by suspending SnCl₄·5H₂O in OLA (10 ml) and heating the suspension at 120 °C under vacuum (5×10^{-2} mbar) for 30 min to yield a transparent solution. Upon cooling to room temperature the solution became cloudy, therefore it was gently heated before use to give a homogeneous, transparent solution. The ZnO:Sn nanocrystal synthesis then proceeded as for the above ZnO:Ge nanocrystal synthesis with the following reagents: Zn(St₂) (2.83 g, 4.48 mmol), DDOL (7.2 g, 38.6 mmol), OA (3.96 g, 14.02 mmol), ODE (12 ml) and Sn precursor solution (4.5 ml). The nominal doping level was 5%, and the sample has been labelled ZSn5.

Instrumentation

Optical absorption spectra of colloidal solutions in TCE and of thin films on glass substrates were measured using a Perkin Elmer Lambda 1050 spectrophotometer in the 300–2500 nm range.

Fourier transform infrared spectroscopy (FTIR) data were collected on a Thermo Scientific Nicolet 6700 spectrometer on a laminated diamond mounted in a stainless steel plate in the 4000–600 cm⁻¹ range with a resolution of 4 cm⁻¹. ZnO-based NCs were drop cast from TCE to form a thin film upon evaporation of the solvent.

X-ray diffraction patterns of the prepared powders were collected using a Bruker D8 diffractometer equipped with a Cu K α radiation source and operated at 40 mV and 40 mA. The crystallite size was evaluated with the Scherrer relationship using the full width at half-maximum obtained by fitting the main nine diffraction peaks detected between 30 and 75° with Lorentzian functions. The resulting crystallite sizes are provided as the average between the values obtained from the nine different peaks, using one standard deviation as error on the measurements.

The chemical composition of the prepared powders was analyzed by XRF. The samples were weighed directly in Pt/Au5% crucibles. The samples were preoxidised with nitric acid and taken to dryness before fusion in lithium borate flux. The resulting glass disks were then presented to the Bruker S8 Tiger WDXRF spectrometer and analysed with a calibration created using synthetic glass standards prepared from pure reagents and lithium borate flux.

Low-resolution transmission electron microscopy (TEM) of colloids deposited on carbon-coated copper grids was performed using a FEI Tecnai 12 G2 microscope operating at 120 kV equipped with an Olympus MegaView III CCD camera. High-resolution TEM was performed using a JEOL JEM 2100F field-emission gun instrument operated at 200 kV, equipped with a Gatan Ultrascan 1000 CCD camera. The JEOL 2100F

microscope has a point resolution of $<2.3 \text{ \AA}$. X-ray energy dispersive spectroscopy (XEDS) was carried out in scanning transmission electron microscopy mode using a JEOL Si(Li) 50 mm^2 detector. The XEDS maps were obtained by collecting ~ 100 frames 256×256 in size with a dwell time of 0.2 msec per pixel and drift correction. Fast Fourier transforms of high-resolution TEM images were performed in Gatan Digital Micrograph using a spherical mask to minimise shape effects.

Scanning electron microscopy (SEM) was performed on a dual beam FEI Helios 600 FIBSEM.

X-ray photoelectron spectroscopy (XPS) analysis was performed using an AXIS Ultra DLD spectrometer (Kratos Analytical Inc., Manchester, UK) with a monochromated Al $K\alpha$ source at a power of 144 W ($12 \text{ kV} \times 12 \text{ mA}$), a hemispherical analyser operating in the fixed analyser transmission mode and the standard aperture (analysis area: $0.3 \text{ mm} \times 0.7 \text{ mm}$) The total pressure in the main vacuum chamber during analysis was typically 10^{-8} mbar. Survey spectra were acquired at a pass energy of 160 eV. High resolution spectra were recorded from individual peaks at 40 eV pass energy. Samples were filled into shallow wells of custom-built sample holders. One lot of each sample was prepared and two different locations were analysed on each sample at a nominal photoelectron emission angle of 0° with respect to the surface normal. Since the actual emission angle is ill-defined in the case of particles (ranging from 0° to 90°) the sampling depth may range from 0 nm to approx. 10 nm.

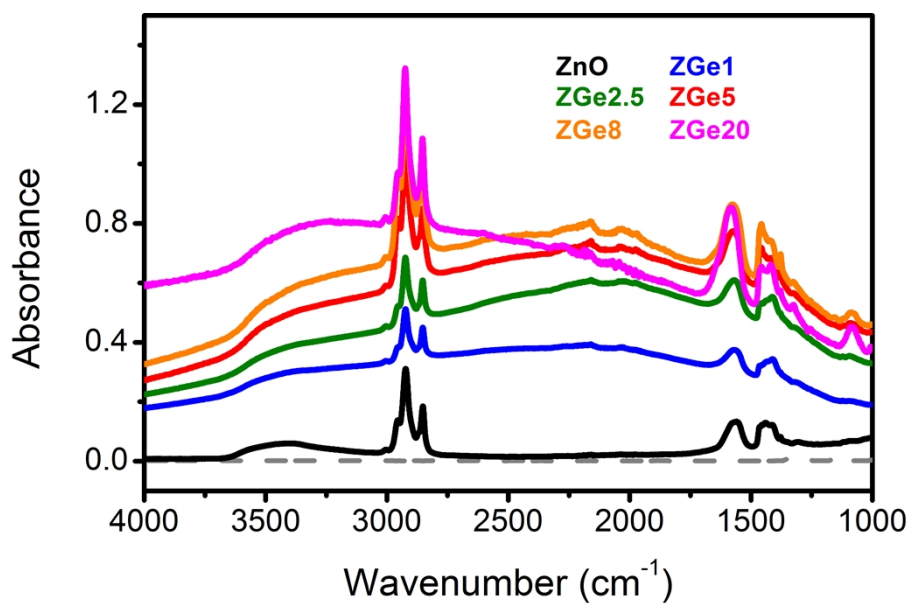


Figure S1. FTIR absorption spectra of the prepared ZnO:Ge colloidal solutions, showing a broad absorption in the near-mid infrared. The dashed grey line is the absorption spectrum of TCE.

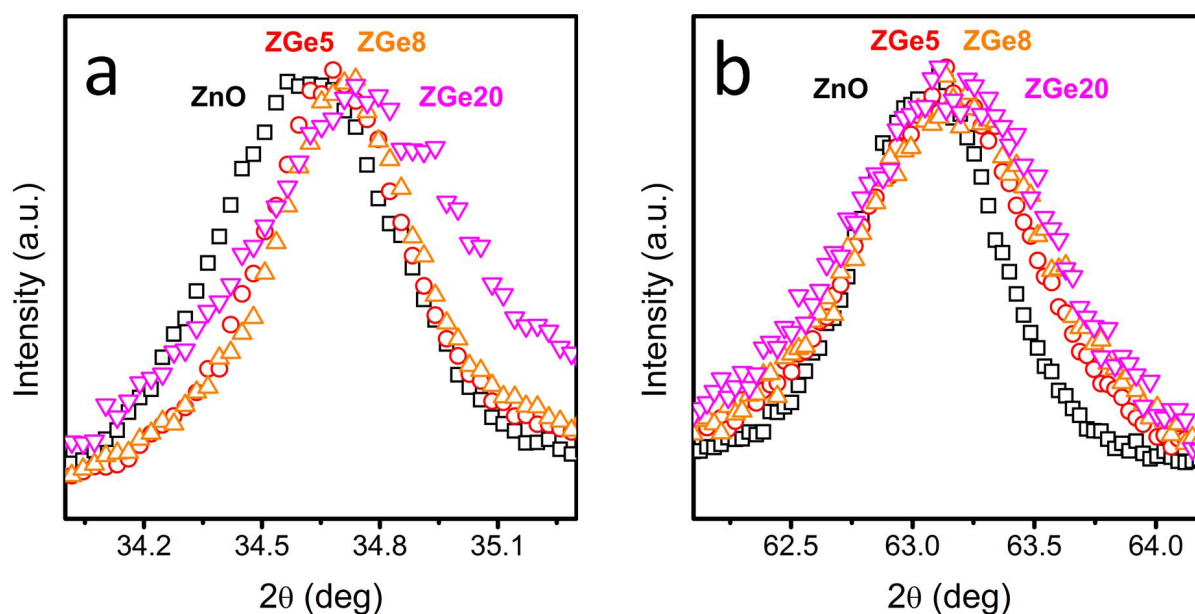


Figure S2. High resolution XRD scans of (a) the (002) and (b) the (103) diffraction peak range for undoped ZnO and Ge-doped ZnO nanocrystal powders. A slight shift towards higher diffraction angles (lower lattice spacing) can be observed, consistent with the substitution of Zn^{2+} with smaller Ge^{4+} metal centers.

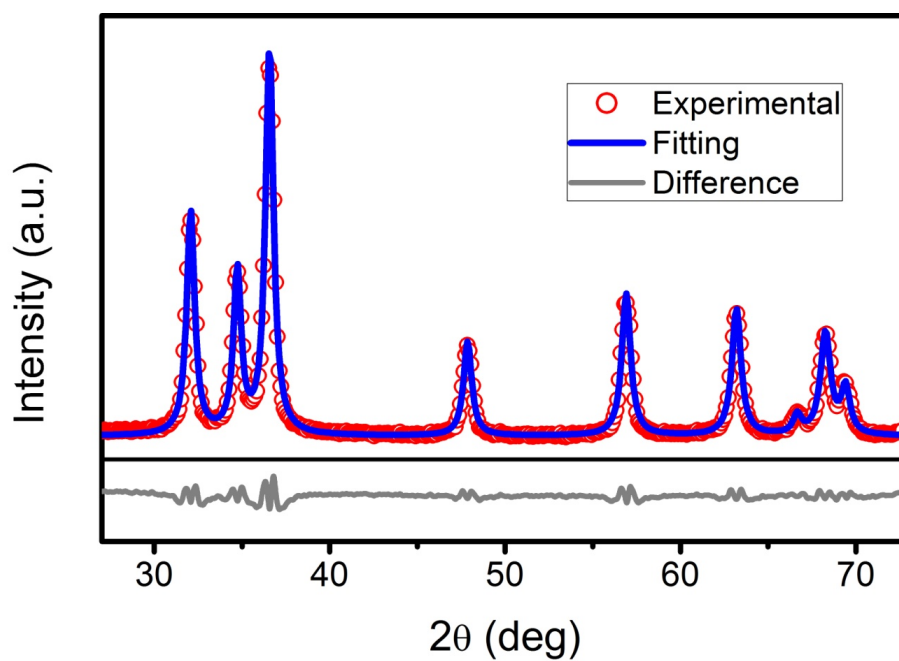


Figure S3. XRD pattern of a typical sample and the sum of the nine Lorentzian functions used to fit the diffraction peaks to estimate the crystallite size.

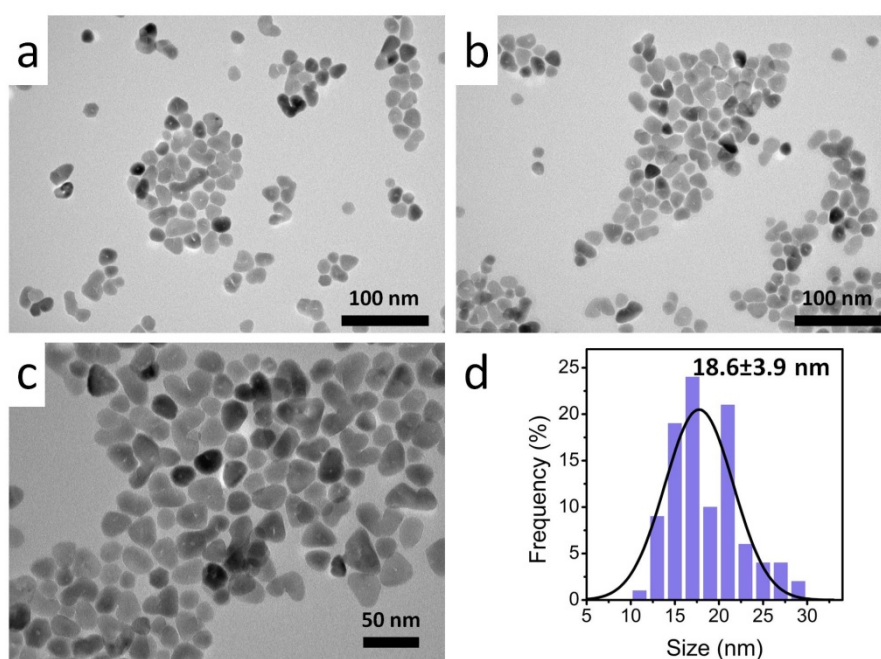


Figure S4. (a-c) TEM images and (d) particle size distribution of ZnO NCs.

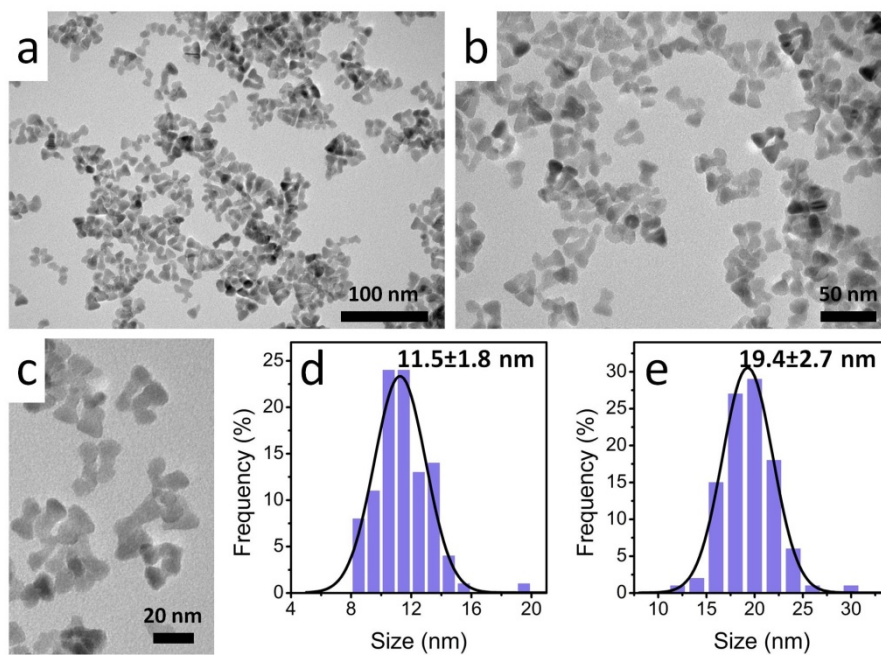


Figure S5. (a-c) TEM images and (d-e) particle size distribution (d, width; e, length) of ZGe1 NCs.

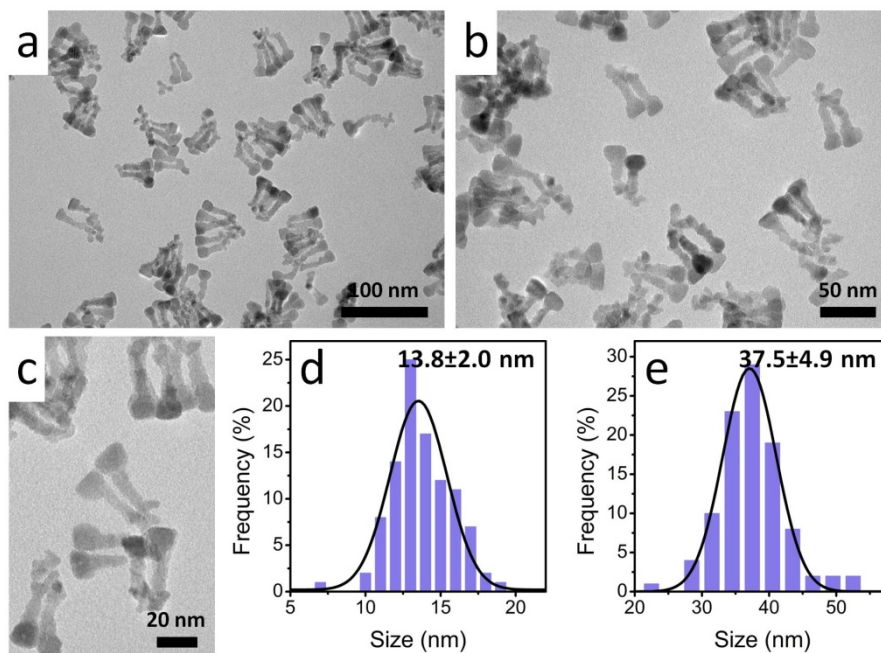


Figure S6. (a-c) TEM images and (d-e) particle size distribution (d, width; e, length) of ZGe2.5 NCs.

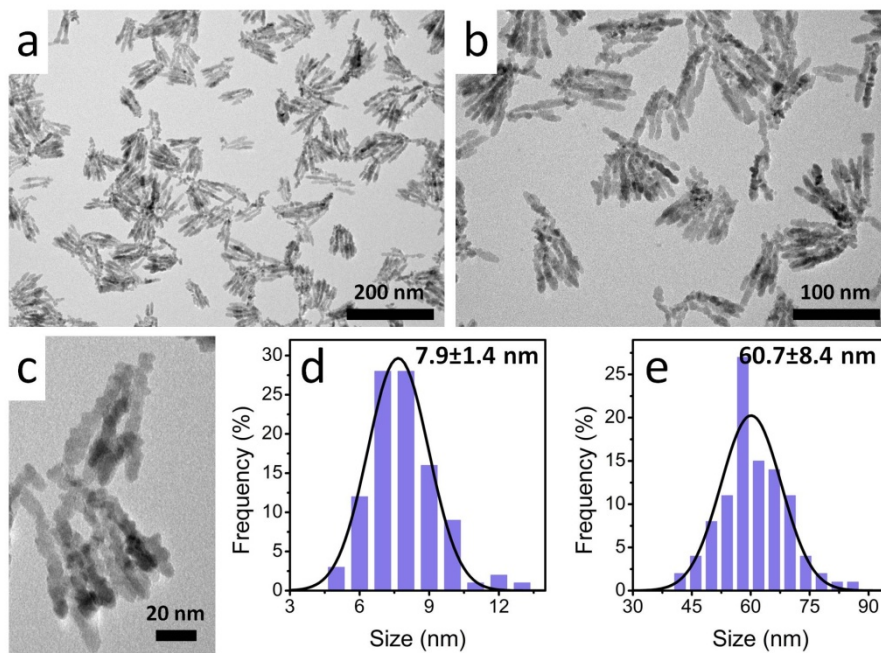


Figure S7. (a-c) TEM images and (d-e) particle size distribution (d, width; e, length) of ZGe5 NCs.

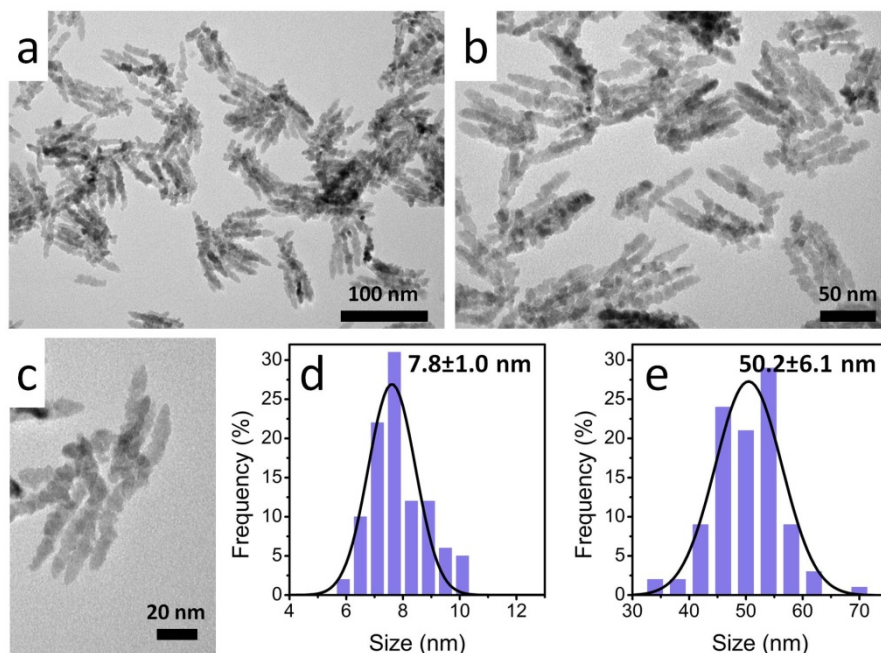


Figure S8. (a-c) TEM images and (d-e) particle size distribution (d, width; e, length) of ZGe8 NCs.

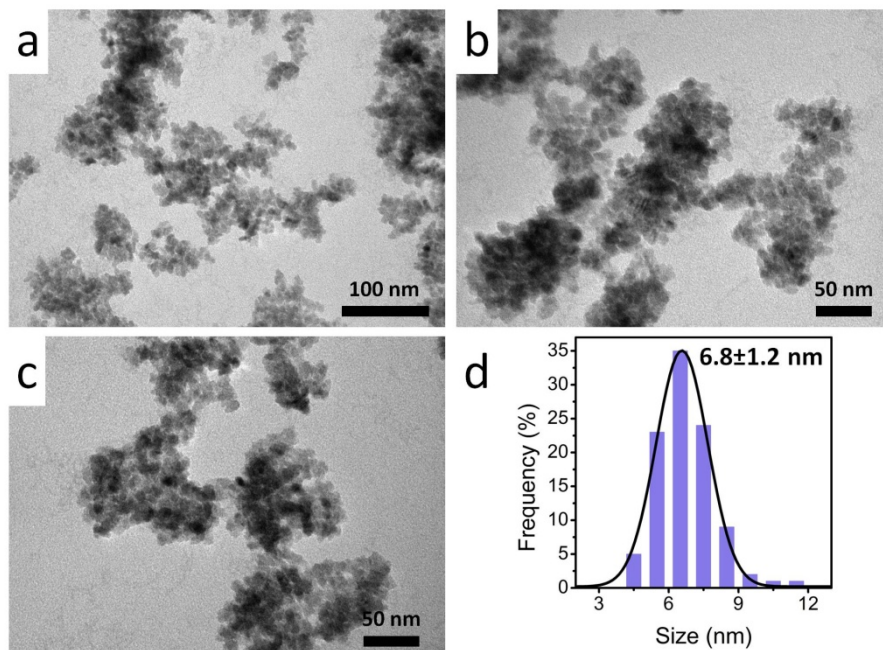


Figure S9. (a-c) TEM images and (d) particle size distribution (d) of ZGe₂₀ NCs.

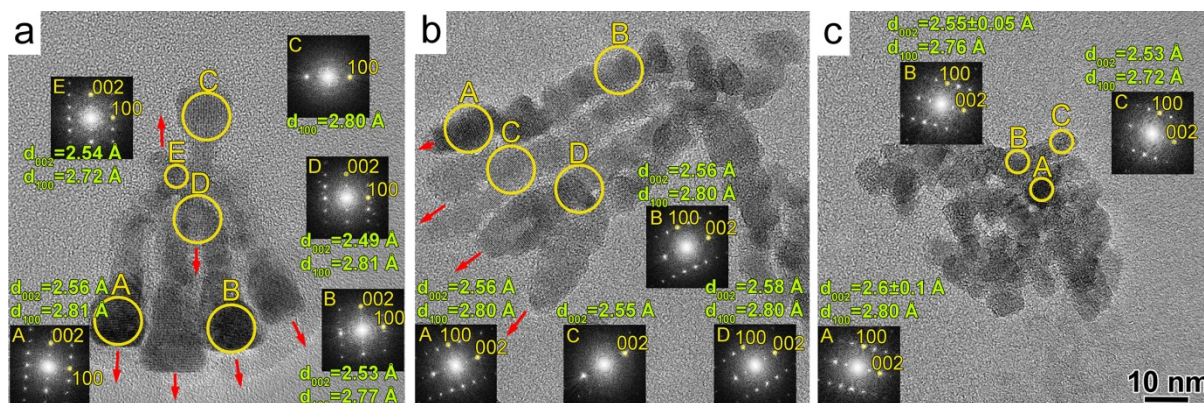


Figure S10. Lattice spacings measured from fast Fourier transforms of the HRTEM images shown in Fig. 3. The measurement uncertainties are $\pm 0.02 \text{ \AA}$ ($\sim 0.7\%$) except where otherwise shown.

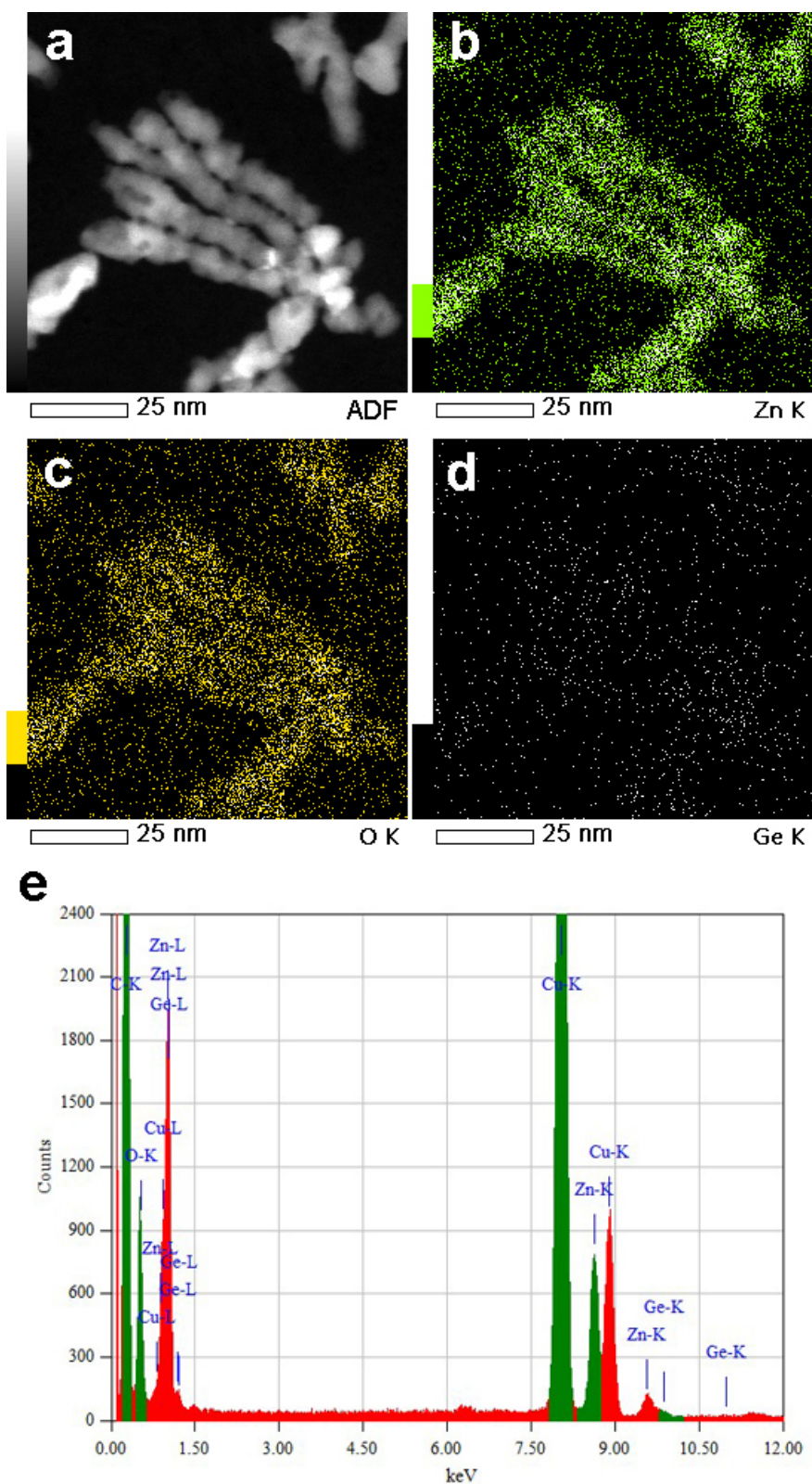


Figure S11. X-ray energy dispersive spectroscopy (XEDS) for a cluster of ZnO:Ge nanorods in the ZGe5 sample. (a) Annular dark field (ADF)-STEM image of the area mapped; (b) Zn map; (c) O map; (d) Ge map; (e) XEDS spectrum for the entire region of interest. Although Ge is clearly detected, it cannot be mapped with confidence due to the overlap between the Ge and the Zn peaks.

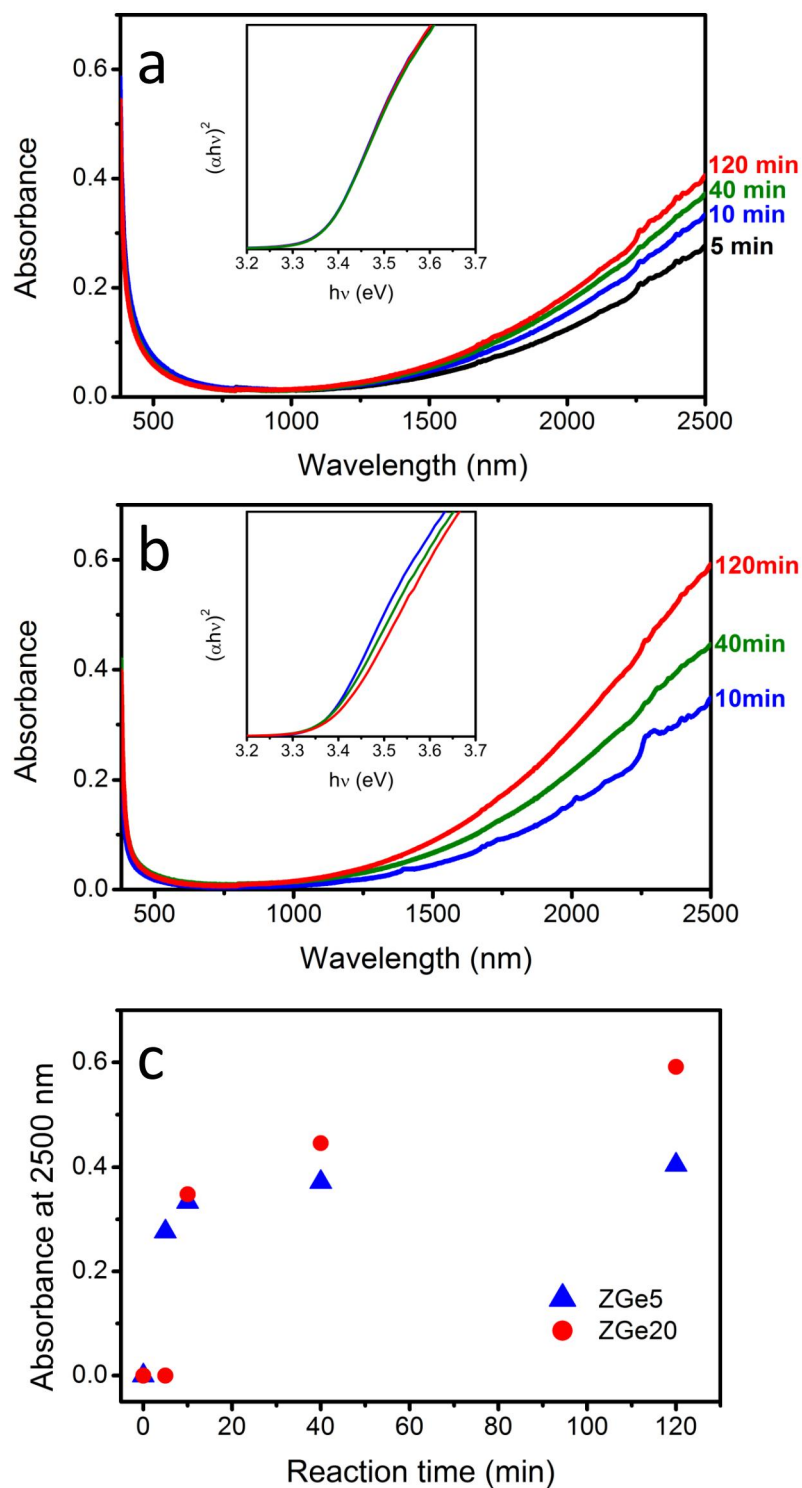


Figure S12. UV-Vis-NIR absorption spectra of (a) ZGe5 and (b) ZGe20 equimolar colloidal solution in TCE as a function of the reaction time. The insets show the respective Tauc plot. c) Plot of absorbance measured at 2500 nm as a function of the reaction time for the two samples.

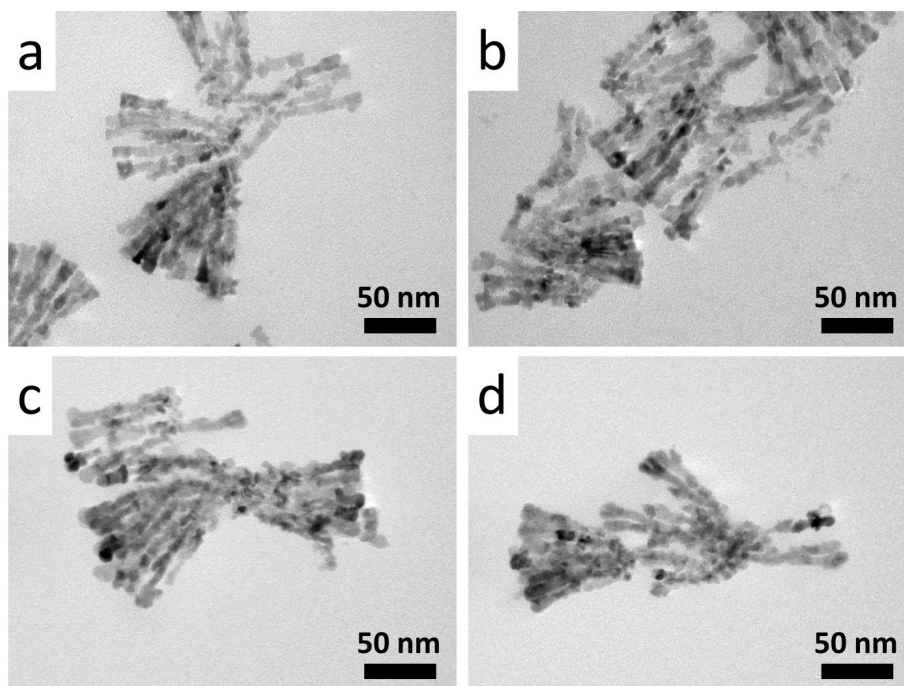


Figure S13. TEM images of ZGe5 NCs synthesized at 230 °C for 10 min (a,b) and 40 min (c,d).

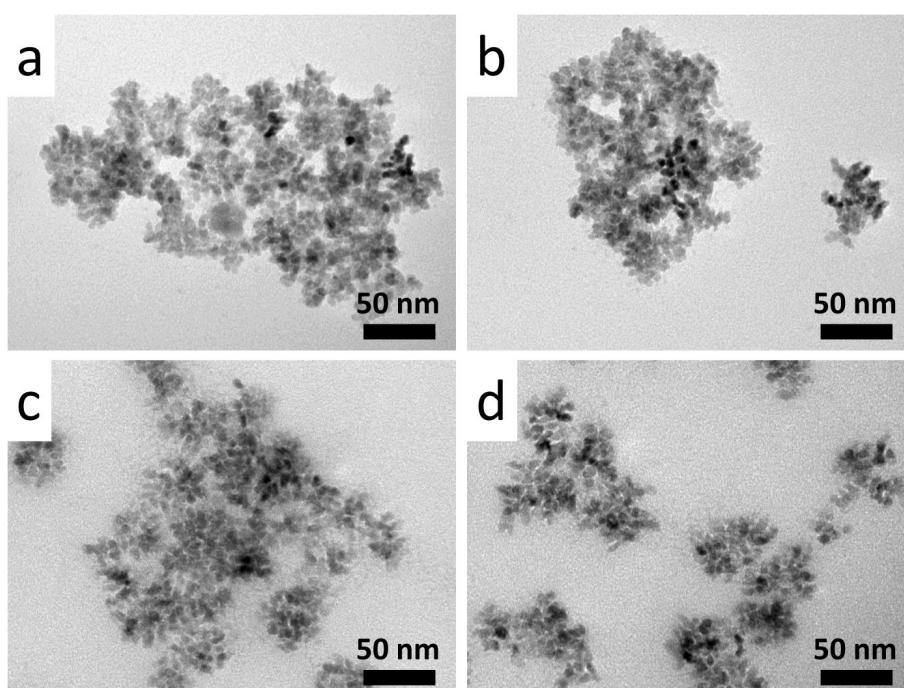


Figure S14. TEM images of ZGe20 NCs synthesized at 230 °C for 10 min (a,b) and 40 min (c,d).

Synthesis and characterisation of Si and Sn doped ZnO

The method presented for the synthesis of Ge-doped ZnO nanocrystals may also be applied to the synthesis of ZnO NCs doped with other p-block elements, namely Si and Sn. Tetraethyl orthosilicate was used as the silicon precursor in the synthesis of ZnO:Si nanocrystals, while $\text{SnCl}_4 \cdot 5\text{H}_2\text{O}$ dissolved in OLA was used as the Sn precursor in the synthesis of ZnO:Sn NCs. The reactant concentrations and solvent ratios were kept constant in the syntheses of Ge, Si and Sn doped ZnO NCs. Doping ZnO with Si proceeded in a similar fashion as to when a Ge precursor was used, with a comparable level of dopant being incorporated into the NCs (Table S1). However, a reduction in the expected intensity of LSPR in the infrared spectrum was observed (Figure S15 a,b). XPS measurements revealed this can be attributed to the Si dopant being predominantly present in the 2+ oxidation state, which causes a reduction the number of free electrons generated, while in the ZnO:Ge NCs the majority of Ge dopant is in the 4+ oxidation state (Figure S16).

Sn had a lower degree of incorporation into the ZnO NCs, with the product displaying a very weak absorption band centered at around 900 nm. While a similar feature was recently identified as an LSPR,³ it is centered at very high energies given the extent of dopant incorporation and the expected free carriers generated in ZnO.⁴ This optical phenomenon (along with the deep blue coloring of the ZnO:Sn nanomaterials Figure 12 e,f) could be due to the presence of SnO impurities, which are known to be highly defective and have a combination of direct and indirect band gaps (2.7 and 0.7 eV respectively) that may generate a dark-blue coloring.^{5,6} However, this hypothesis could not be confirmed by XRD as no impurity phases were detected, or XPS as we could not distinguish clearly between Sn^{2+} and Sn^{4+} , due to their close respective binding energies (Figure S16e). Further investigations are needed to address this point, which is outside of the scope of the current study.

TEM analysis of the Si doped ZnO NCs reveals that they have the same distinctive morphology as that observed in ZnO:Ge NCs when Ge is incorporated as a dopant at the same concentration (Figure S17). Tin does not have such an effect, with ZnO:Sn NCs being isotropic and very similar in morphology to undoped ZnO NCs, with only an increased average size observed (Figure S18). However, levels of Sn inclusion comparable to those achieved for Si and Ge dopants were not reached in this study.

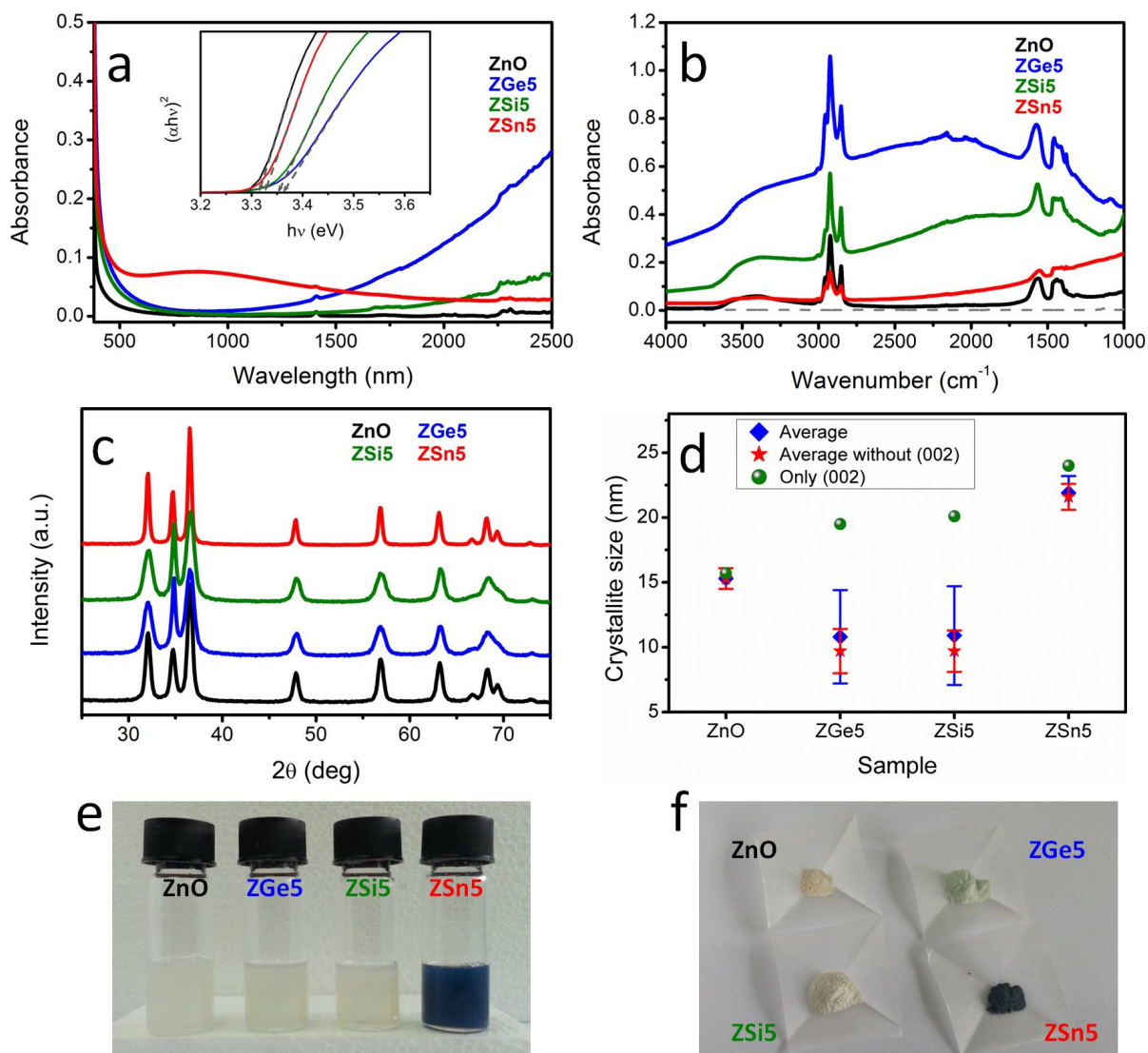


Figure S15. Characterization of ZnO NCs doped with Si, Ge and Sn. (a) UV-Vis-NIR absorption spectra of equimolar colloidal solutions in TCE. The inset shows the respective Tauc plot. (b) FTIR absorption spectra. (c) XRD patterns. (d) Crystallite size evaluated from the diffraction patterns. (e) Digital photographs of colloidal solutions. (f) Digital photographs of dry powders.

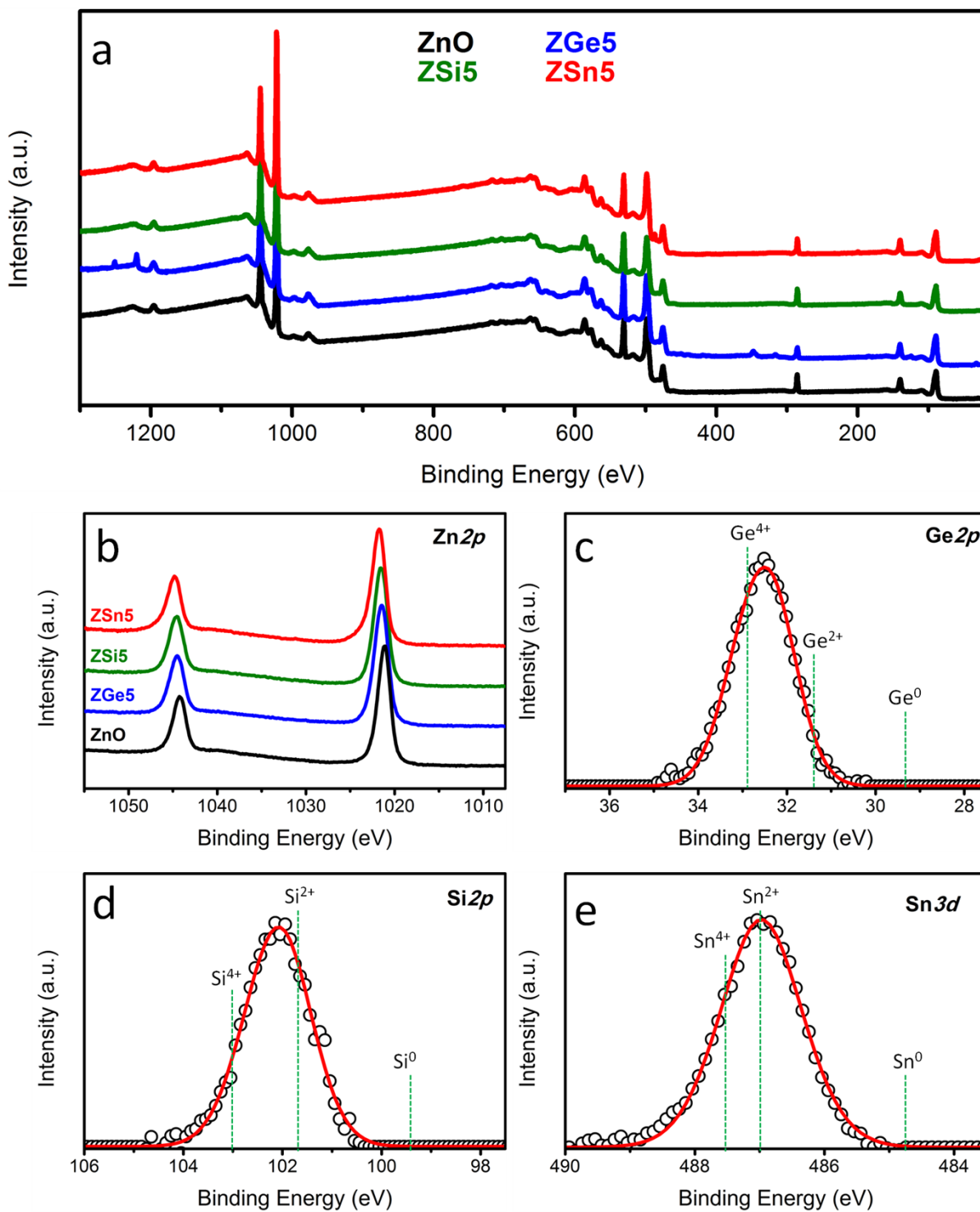


Figure S16. X-ray photoelectron spectra (XPS) of (a) survey of all samples; (b) Zn $2p$ region of all samples; (c) Ge $2p$ region, (d) Si $2p$ region and (e) Sn $3d$ region for ZGe5, ZSi5 and ZSn5 samples, respectively.

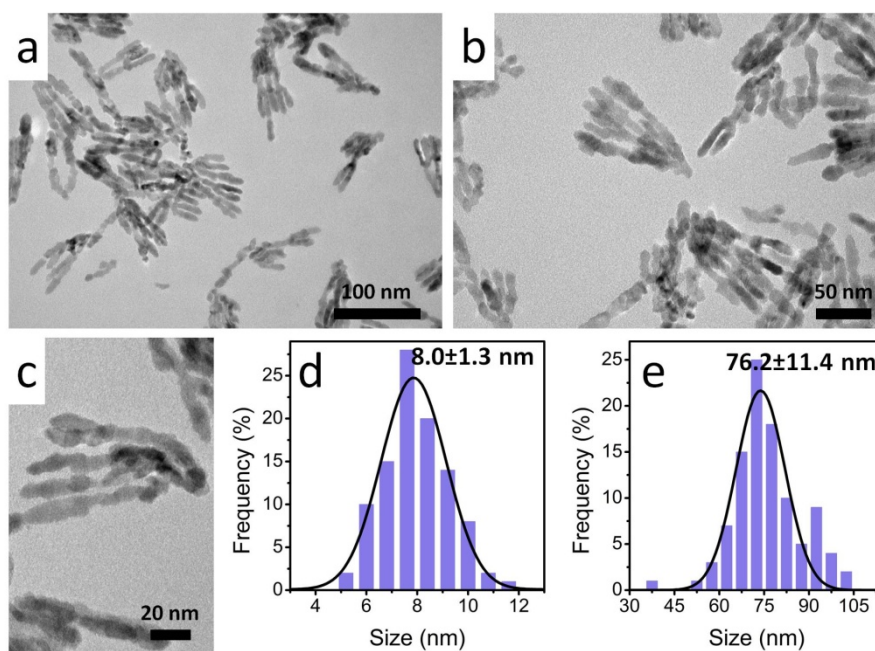


Figure S17. TEM images (a-c) and particle size distribution (d, width; e, length) of ZSi5 NCs.

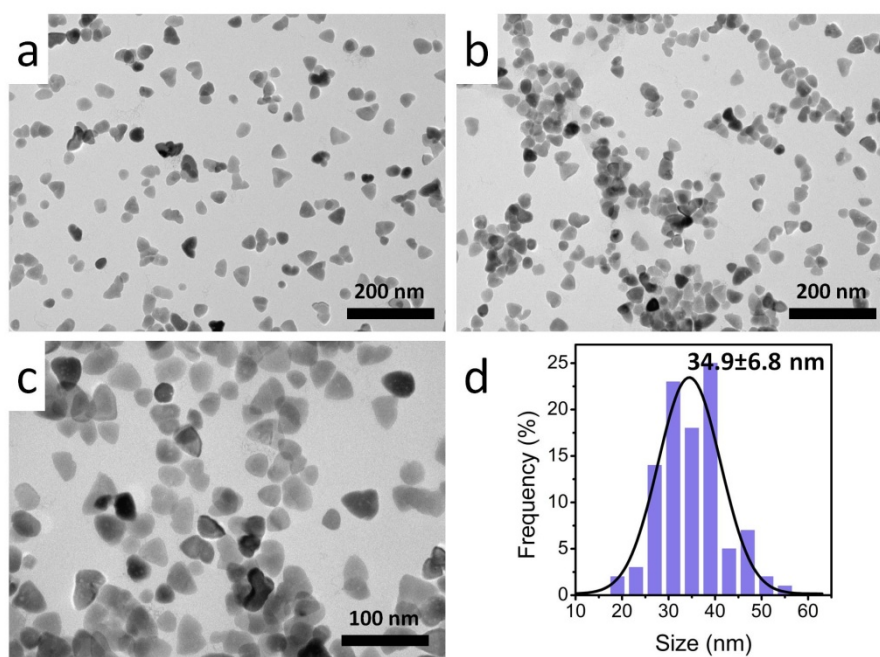


Figure S18. TEM images (a-c) and particle size distribution (d) of ZSn5 NCs.

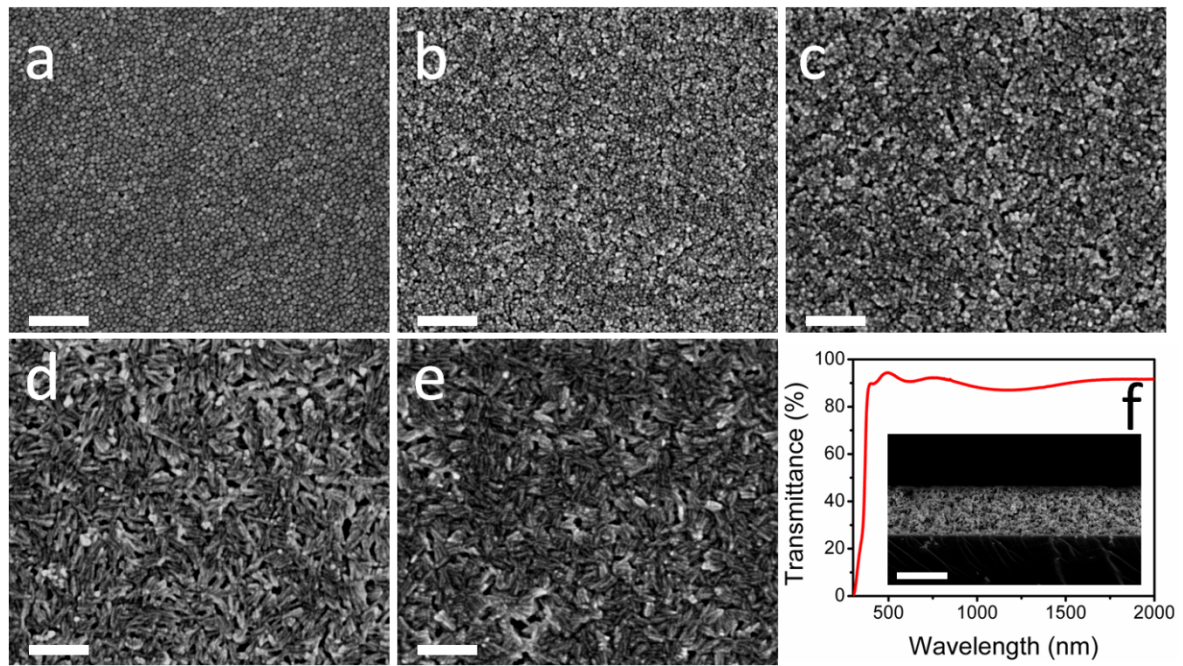


Figure S19. (a-e) SEM images in top view of ZnO:Ge NC thin films: (a) ZnO, (b) ZGe1, (c) ZGe2.5, (d) ZGe5 and (e) ZGe8. (f) Optical absorption spectrum and (inset) SEM image in cross section of a ZGe5 NC thin film. The scale bars are 200 nm in panels a-e and 500 nm in panel f.

Table S1. List of the prepared samples highlighting the type of dopant, its nominal amount and the real doping level evaluated from XRF measurements.

Sample label	Dopant	Dopant/Zn precursor loading (atomic %)	Dopant/Zn in the synthesized powders (atomic %)	Doping efficiency (real dopant vs. expected dopant)
ZnO	-	0	0	-
ZGe1	Ge	1	0.72	72%
ZGe2.5	Ge	2.5	1.88	75%
ZGe5	Ge	5	3.70	74%
ZGe8	Ge	8	6.26	78%
ZGe20	Ge	20	10.2	51%
ZSi5	Si	5	4.12	82%
ZSn5	Sn	5	0.85	17%

References

- (1) Chesman, A. S. R.; van Embden, J.; Della Gaspera, E.; Duffy, N. W.; Webster, N. A. S.; Jasieniak, J. J. *Chem. Mater.* **2014**, *26*, 5482-5491.
- (2) Chiang, H.-C.; Wang, M.-H.; Ueng, C.-H. *Acta Crystallogr., Sect. C* **1993**, *49*, 244-246.
- (3) Ghosh, S.; Saha, M.; Dev Ashok, V.; Dalal, B.; De, S. K. *J. Phys. Chem. C* **2015**, *119*, 1180-1187.
- (4) Lounis, S. D.; Runnerstrom, E. L.; Llordés, A.; Milliron, D. J. *J. Phys. Chem. Lett.* **2014**, *5*, 1564-1574.
- (5) Ogo, Y.; Hiramatsu, H.; Nomura, K.; Yanagi, H.; Kamiya, T.; Hirano, M.; Hosono, H. *Appl. Phys. Lett.* **2008**, *93*, 032113.
- (6) Sakaushi, K.; Oaki, Y.; Uchiyama, H.; Hosono, E.; Zhou, H.; Imai, H. *Nanoscale* **2010**, *2*, 2424-2430.